Deep spallation of medium mass isotopes by protons

Kathryn L. Kolsky
Medical Department, Brookhaven National Laboratory, Upton, New York 11973

Paul J. Karol
Department of Chemistry, Carnegie Mellon University, Pittsburgh, Pennsylvania 15213

(Received 28 December 1992)

Spallation systematics have been extended into the deep spallation mass region. Production cross sections of scandium radioisotopes from 0.8 GeV protons on ^{89}Y, ^{92,96,100}Mo, and ^{130}Te targets were measured and the cross sections were used to generate isobaric yield curves at $A_p=47$. In the latter target, this corresponds to a mass loss of >80 nucleons. At ~ 10 MeV/nucleon and for products outside the multifragmentation region, this is an extreme manifestation of the spallation process. The results prove to fit smooth extrapolations from trends developed in earlier work on less deep spallation. The influence of target composition is still evident even from ^{130}Te, in contrast to expectations, based on evaporation considerations, that this so-called memory effect would wash out.

PACS number(s): 24.90.+d, 25.40.−h, 25.40.Sc

I. INTRODUCTION

Spallation is a high-energy nuclear reaction process described by the widely used Serber two-step model [1,2]. A fast projectile interacts with a target nucleus through nucleon-nucleon collisions, causing the ejection of a number of nucleons or nucleon clusters leaving a residue frequently at high temperature. Even in heavy-ion collisions, the two-body dynamics are evident at energies as low as 30 MeV/nucleon as evidenced, for example, by high-energy gamma measurements explained in terms of proton-neutron brehmsstrahlung [3] and also by interpretation of total reaction cross sections [4]. The fast step's residue is left with excess internal energy associated with particles and holes and deexcites, via evaporation of nucleons, light clusters such as alpha particles and, less frequently, heavier fragments [2,5]. An elegant prescription for the two-step spallation model reproduces general features observed in experiments [6]. Statistical models of evaporation depend on the nuclear equation of state, which is of considerable fundamental interest, especially at high temperatures. The crossover between the two reaction steps in spallation depends on the time scales involved, which are also the subject of much attention and debate. The cross section values themselves are of interest because of applications to the production of exotic secondary beams far from stability, to the understanding of the propagation of cosmic rays through interstellar media, and to determinations of cosmic-ray source elemental and isotopic composition.

Hüfner [7] characterized spallation as high-energy reactions leading to products with masses down to half of the target mass. Residual product mass distributions from high-energy reactions show product yields decreasing rapidly and basically exponentially with increasing mass loss until the product mass number reaches approximately 40. Observed production of still lighter products have their formation attributed to a fragmentation or multifragmentation mechanism. Fragmentation yields for mass numbers <40 increase with ΔA and have contributions from both fast and slow time domains during the spallation process.

The spallation process has frequently been characterized by activation studies which provide an isobar cross section's dependence on its charge Z, i.e., the isobaric charge distribution. Alternatively, the distribution variable can be (N/Z) or (Z_A-Z). In more recent years, isotopic distributions have been measured by nonactivation methods. Peak maxima for all but the lightest of products lie on the neutron-deficient side of stability and fall off sharply on both sides, reflecting the dominant role of the nuclear mass-energy surface in favoring evaporations that drive residual nuclei toward stability [8].

Interpretation of activation measurements was carried a step further by Ku and Karol [9]. They analyzed $A_p=72$ isobaric distributions from the interactions of 0.72 GeV alpha particles with ^{92,96,100}Mo targets and found that not only the most probable product composition, but also the distribution width itself varied in a smooth fashion with target composition. Tobin and Karol [10] extended the studies of $A_p=72$ isobaric charge distributions, measuring product yields from the interactions of 0.8 GeV protons with ^{89}Y, ^{92,96,100}Mo, and the very neutron-rich ^{130}Te. These nuclides provide a large variation in target neutron-to-proton ratios. The study enabled comparison of proton-induced spallation at 0.5, 0.8, and 2.9 GeV and of protons with alphas as incident projectiles. Very recent studies with relativistic heavy ions enable such comparisons to be expanded still further [11].

The principal motivation of the current work was to expand the spallation systematics our group has developed into the very deep spallation region where almost no measurements have been made other than from heavy targets in which the contribution from high-energy fission can significantly confound interpretation. In order

to facilitate comparisons with the shallower results referenced above, the target nuclides employed in this study were identical to those chosen by Tobin and Karol [10], ^{89}Y, ^{92,96,100}Mo, and ^{130}Te. Yields of Sc products in the mass region $43 \leq A_p \leq 48$ were measured. The products are arguably beyond the fragmentation region ($A_p \leq 40$). Furthermore, the associated mass loss from the various targets places them in the deep spallation region, $41 \leq \Delta A \leq 87$. Based on high-energy fission systematics [12], discussion of their production at 0.8 GeV is not expected to be complicated by contributions from fission.

II. EXPERIMENTAL DETAILS

Irradiations were performed at the Los Alamos Meson Physics Facility (LAMPF) at Los Alamos National Laboratory, using the 0.8 GeV external H^- beam. Irradiation times were 8–15 min for absolute cross section measurements and 30 min for relative yield determinations. The beam intensity ranged between 1 and 6 μA.

The ^{92,96,100}Mo and ^{130}Te targets employed in this study were made from enriched powdered metal isotopes, $\geq 96\%$ pure, obtained from Oak Ridge National Laboratory. Natural ^{89}Y targets were 25 μm metal foil, 99.999% pure. For the Mo and Te targets, self-supporting 1.50×2.00 cm^2 target pellets containing 30–50 g/cm^2 of enriched target isotope and boric acid serving as a binder were prepared using a 20-ton hydraulic press [13]. The absolute yield targets consisted of a stack of two 25 μm ^{27}Al foils serving as the monitor and catcher, the target pellet or foil, and a final 25 μm ^{27}Al catcher foil. The target stacks were carefully aligned and sealed in a 100 μm Al guarding envelope. Several blank targets containing only binder were also irradiated to confirm the absence of contribution from the boric acid itself. In some cases, the enriched metals were converted to water-soluble solids [14]—$(NH_4)_2MoO_4$, $TeO_3(OH)NO_3$, $Y(NO_3)$—prior to irradiation to facilitate rapid radiochemical separations after bombardment.

After irradiations, radiochemical separations, developed from standard precipitation, solvent extraction, and ion-exchange techniques, were performed. The relevant decay properties of the Sc nuclides were taken from Lederer and Shirley [15]. All targets and monitors were counted with calibrated Ge(Li) and high-purity Ge detectors. The monitor and all of the Sc isotropic decay curves, except ^{44}Sc^{m,g}, were analyzed by a weighted linear least-squares program CLSQ [16] to determine end-of-bombardment activities and their uncertainties. ^{44}Sc^{m,g} growth and decay curves were analyzed with a nonlinear least-squares program NLREG [17]. Chemical yields were determined spectrophotometrically [18]. Further details are available in Ref. [19].

III. RESULTS

All experimental cross sections were measured relative to the ^{27}Al$(p,x)^{24}$Na monitor reaction (10.5±0.5 mb) [20] at 0.8 GeV. The experimentally determined spallation cross sections are presented in Table I. Each cross section is identified as either independent (I) or virtually independent ($\underline{I}$) if the estimated contribution from the precursor is minor. The reported values are the average of two or three independent determinations. The cross sections were corrected for coincidence summing losses and for contributions from the minor target isotopic impurities. No correction was attempted for scattering effects since previous studies employing identical targets showed these corrections to be negligible [10].

The uncertainty associated with each cross section value represents the total experimental uncertainty calculated from the associated systematic and random uncertainties. The systematic uncertainties considered were the counter efficiencies, decay schemes, monitor cross section value, minor target isotopic impurity corrections, and summing corrections. The sources of random uncertainty were counting statistics, decay curve analyses, chemical yield determinations, timing, and target misalignment. Any contributions to the ^{24}Na monitor cross section from secondary particles produced within the target were assumed to be insignificant based on previous work [14,21,22].

Isobaric yield curves. A major objective of this study at $A_p = 47$ was to explore deep spallation particularly in comparison to the detailed spallation systematics developed from less deep spallation products at $A_p = 72$. As discussed below, mass loss from the target is a natural way of binning the results. Therefore, as a first step in the analysis, Z dispersions at fixed mass loss, familiarly called "charge distribution curves," were determined from the experimental data. Subsequently, the appropriate mass-loss distributions or mass-yield curves were derived.

The isotopic cross section measurements reported in Table I are by themselves not sufficient to permit a detailed determination of the charge distribution curves.

TABLE I. 0.8 GeV proton-induced spallation cross sections (μb).

Nuclide	N/Z	^{89}Y	^{92}Mo	^{96}Mo	^{100}Mo	^{130}Te
^{43}Sc $\underline{I}$[a]	1.0476	99.0±11.9	116±14	48.8±6.6	17.2±3.5	5.6±1.5
^{44}Sc^m I	1.0952	374±39	356±39	195±23	99.6±12.9	21.9±2.6
^{44}Sc^g I	1.0952	238±29	200±26	107±15	52.5±7.8	10.0±1.5
^{46}Sc I	1.1905	733±110	428±73	328±54	251±31	51.2±16.6
^{47}Sc I	1.2381	338±37	180±24	167±21	140±18	31.9±4.6
^{48}Sc I	1.2857	114±15	46.0±5.1	56.1±7.8	63.2±8.0	16.5±2.9

[a] $\underline{I}$, virtually independent.

However, isobaric yield curves may be constructed from cross sections spanning a range of mass numbers close to the chosen isobar from iterative fits of mass-yield corrected data to a continuous model distribution. The detailed data generated by previous studies [9,10] showed that isobaric distribution shapes can be described by a skewed Gaussian function. The four-parameter skewed Gaussian distribution shape chosen to fit the present experimental data was developed from a normal cumulative distribution [23] written here in terms of the standardized variable $t=(x-\mu_1)/\sigma$.

$$P(t)=P_0 e^{-t^2/2}\left[1+\frac{\mu_3'}{6\sigma^3}(t^3-3t)\right] . \quad (1)$$

This distribution is totally characterized by P_0, μ_1, σ, and μ_3', respectively, the curve maximum, the mean, the standard deviation $[(\mu_2')^{1/2}]$, and the third central moment. The latter is related to the skewness of the distribution, γ_1, by $\gamma_1=\mu_3'/\sigma^3$. For the variable in the charge distribution curves, we prefer to use N/Z rather than Z_A-Z because the latter is much more subject to arbitrariness over how to incorporate shell effects.

Experimental data from Table I were adjusted to isobaric results at $A_p=47$ with the following assumptions based on our previous spallation studies [9,10,22].

(1) The shapes, but not the absolute magnitudes, of isobaric curves over narrow mass ranges may be represented by one set of parameters. It is then possible to adjust the cross sections of nuclei in the surrounding mass region to a given isobaric distribution if information is available concerning the ΔA or A_p dependence of the total isobaric yield (mass yield) over the mass region of interest.

(2) Beyond the mass region a few nucleons removed from the target, mass yields of spallation products, $Y(A_p)$ decrease exponentially with increasing mass loss from the target, $Y(A)\propto\exp(-p_T\Delta A)$ [5,24]. p_T is the mass-yield coefficient for the particular target/projectile/energy combination, i.e., the logarithmic slope of the appropriate mass-yield curve.

For each target, the appropriate mass-yield coefficient p_T was determined by successive approximation. The experimental data reported by Ku and Karol [9] and Tobin and Karol [10] indicate an average mass-yield slope of approximately 10%/nucleon for 0.8 GeV protons and medium mass targets. As an initial guess, the isotopic cross sections were corrected to the $A_p=47$ isobaric curve using $p_T=0.1$. Statistical moment calculations were performed on these corrected yields to provide initial shape parameter estimates with which to fit Eq. (1) using the nonlinear least-squares program NLREG [17]. The refined shape parameters were used to generate a "universal" isobaric curve shape. Using the latter, isobaric distributions for masses $43\leq A_p\leq 48$ were generated at each mass number and the curves were normalized to the experimentally measured isotopic cross section at the given mass number. Next, mass yields $Y(A_p)$ for each such A_p curve were determined by summing the measured and extrapolated isobaric cross sections. An error of 20% of the extrapolated yield was included with the error of the measured yield to give the uncertainty of the total isobaric yield. In previous work [10] first-pass mass yields were used to optimize the mass-yield coefficient by fitting to the equation $\ln Y(A_T)=b+p_T(A-A_p)$. However, for these scandium results this alone will not work because the mass yields here span a much narrower mass region, five isobars, than that spanned by the data of Tobin and Karol, 20 isobars, for example. Since the target/projectile combinations Tobin and Karol used were identical to those in the present study, the spallation data at $65\leq A_p\leq 83$ were included in the interactive regression procedure for p_T down to $A_p\simeq 47$.

The optimal mass-yield coefficients and the associated uncertainties for all of the targets studied are listed in Table II. Figure 1 shows mass yields from the present study (solid circles) and from Tobin and Karol [10] (open circles). The solid line is from a linear regression of the logarithmic data. The magnitudes of the mass-yield coefficients are very comparable to results previously published at projectile energies near 0.8 GeV [9,10], but for the first time, they are shown to extend to much greater mass losses in spallation. The lingering question of whether the mass-yield slope coefficients at $A_p\simeq 47$ have been obtained through circular arguments will be addressed in subsequent discussion.

The mass-yield-adjusted $A_p=47$ isobaric curves for the five isotopic targets are plotted as a function of product composition in Fig. 2. The error bars reflect the uncertainties listed in Table I as well as the estimated uncertainties associated with the iterative mass-yield corrections themselves. The solid curves represent the optimal skewed Gaussian fits to the experimental data.

Figures 2(a)–2(e) show that the yields decrease with increasing mass loss from the target, in a manner completely consistent with spallation systematics at smaller ΔA [9,10,22,25,26]. The distributions peak at $N/Z\sim 1.17$, slightly, but significantly, to the neutron-deficient side of

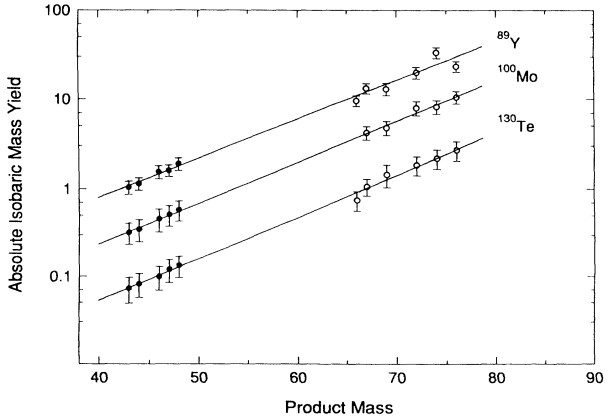

FIG. 1. Mass-yield distributions for the interaction of 0.8 GeV protons with ^{89}Y, ^{100}Mo, and ^{130}Te targets. Solid circles, yields determined from this work; open circles, determined from Tobin and Karol [10]; solid lines are linear regressions of the data.

TABLE II. Logarithmic mass-yield slopes at 0.8 GeV for $40 \leq A_p \leq 80$.

Target	Mass-yield slope, P_T
^{89}Y	0.099± 0.020
^{92}Mo	0.108± 0.016
^{96}Mo	0.100± 0.034
^{100}Mo	0.113± 0.021
^{130}Te	0.108± 0.008

stability at $(N/Z)_A = 1.193$ [27], corresponding to a few tenths of a charge unit shift. The curves are asymmetric and skew out to the neutron excessive sides. Figure 2(f) shows the superimposed isobaric distributions rescaled to the ^{89}Y maximum yield for visual comparison. Displayed in this manner, the figure clarifies two trends tracking increasing target N/Z: a shift in the position of the peak maximum toward higher product N/Z and an increase in the widths of the distributions.

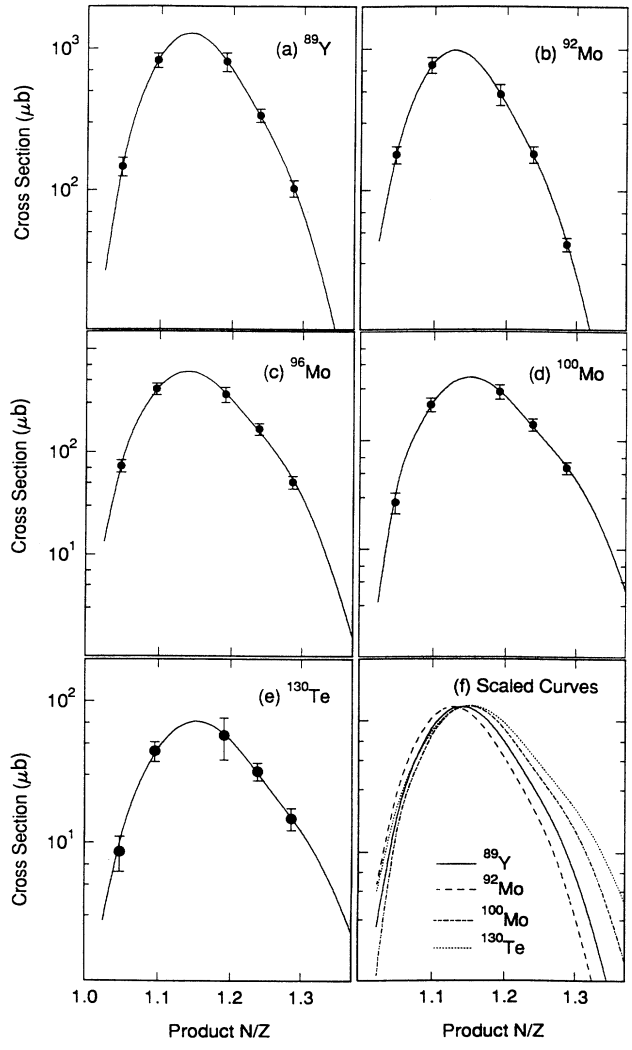

FIG. 2. $A = 47$ absolute isobaric curves from the interaction of 0.8 GeV protons with ^{89}Y, ^{92,96,100}Mo, and ^{130}Te targets. Solid curves through data are fits to Eq. (1).

IV. DISCUSSION

A. Semi-empirical parametrizations

Over the years, smooth empirical functions have been fit to experimental mass and charge yields as a means to summarize a wide variety of spallation data and also to interpolate unknown cross sections. Proton-induced spallation cross sections are generally estimated using an empirical relationship based on variations of Rudstam's original expression [24].

$$\sigma(Z, A) = f(A_T, E)\exp[PA - R|Z - SA + TA^2|^{\alpha}] , \quad (2)$$

where $\sigma(Z, A)$ is the predicted isobaric cross section, A_T is the target mass number, E is the projectile energy, and

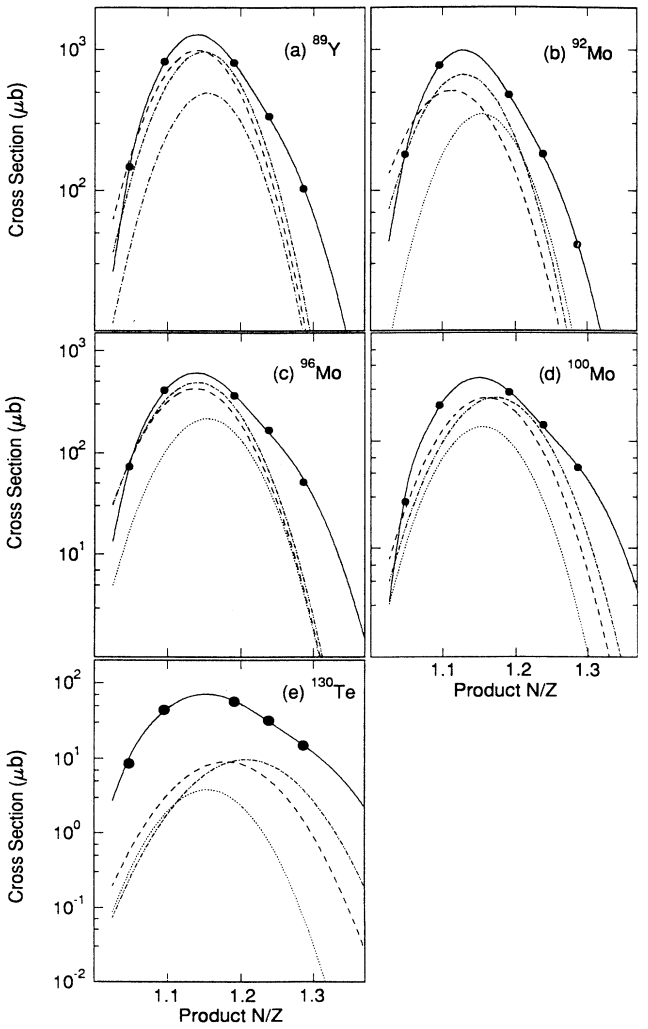

FIG. 3. Comparisons of fitted skewed Gaussian distribution curves (solid curves) from Eq. (1) with semiempirical estimates for ^{89}Y, ^{92,96,100}Mo, and ^{130}Te targets. Dashed curves, Silberberg *et al.* [31,32]; dotted curves, Rudstam [29]; dot-dot-dashed curves, Chackett and Chackett [30].

$f(A_T,E)$ is related to the total inelastic cross section. Information from a wide range of spallation studies was condensed into a few empirical parameters (S, T, P, and R). The parameter P is analogous to the mass-yield coefficient, R governs the width of the product isobaric distributions, and the parameters S and T jointly define the most probable peak position. Equation (2) was modified by Chackett and Chackett [30] and also by Silberberg *et al.* [31,32] to account for the target composition influence on the peak of the product distributions. Sümmerer *et al.* [29] have reexpressed the target dependence in a different form. For isotopic distributions, Webber, Kish, and Schrier [11] devise a somewhat different expression more indicative of their recent, higher-precision heavy-ion results.

Figure 3 shows isobaric curves for $A_p=47$, estimated from the semiempirical relationships [24,30–32] using the computer program SPALL [33]. In order to facilitate curve comparisons, the isobaric yields calculated from the present experimental data (solid circles) and their fitted curves (solid lines) are also provided. The equations of Chackett and Chackett [30] and Silberberg *et al.* [31,32], as expected, both reproduced a shift in peak position with target composition. However, none of the semi-empirical formulas accommodate a shift in the width or asymmetry of the curves with increasing target N/Z. In fact, Sümmerer *et al.* [29] in their study of relativistic heavy-ion spallation, believe their data confirm that the width is constant. In most comparisons, even the magnitudes of the distribution widths are not qualitatively reproduced. All three of the formulas severely underestimate the curve widths of the neutron-rich targets ^{100}Mo and ^{130}Te. The magnitudes of the spallation yields from Y and Mo are reproduced adequately. However, the ^{130}Te deep spallation yields predicted by the Rudstam and Chackett-Chackett equations are an order of magnitude lower than the experimentally measured yields. The equation of Silberberg *et al.* in contrast, anticipates higher yields from ^{130}Te due to the inclusion of contributions from breakup and fission which are apparently overestimated for the relatively nonfissile ^{130}Te.

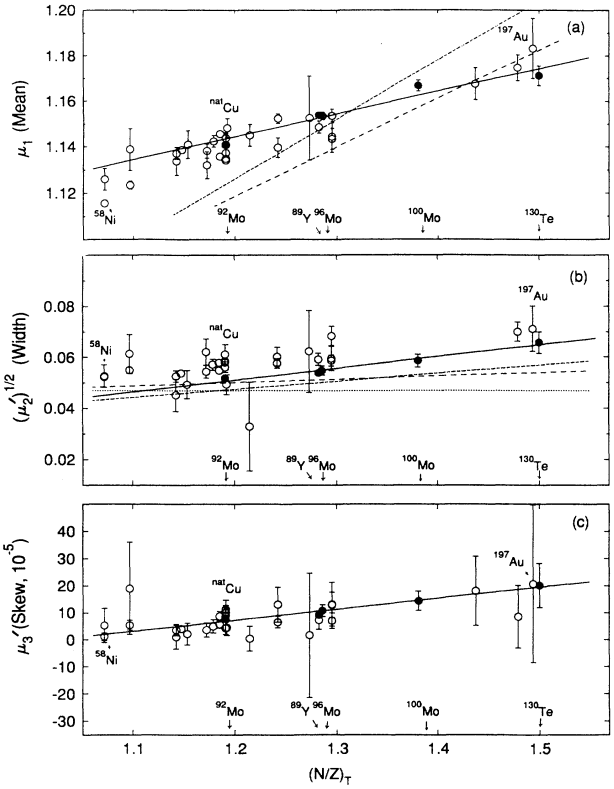

FIG. 4. Variation of isobaric yield curve shape parameters with target composition (N/Z). Solid curves and closed circles, present work; open circles, data listed in Table IV analyzed with Eq. (1). Semiempirical analysis: dashed curves, Silberberg, *et al.* [31,32]; dotted curve, Rudstam [29]; dot-dot-dashed curves, Chackett and Chackett [30].

B. Fitted shape parametrizations of isobaric curves

The shape parameters, determined from fitting the $A_p=47$ isobaric curves to Eq. (1), are listed in Table III. Shown in Figs. 4(a)–4(c) is the target composition dependence of these parameters, that is, the increasing values of the shape parameters with increasing neutron excess in the targets. These trends have not been reported previously for spallation reactions leading to such large mass losses, $\Delta A>60$, where fission contributes little. At this point, justification for the iterative method employed to determine the mass-yield coefficient p_T, operative at $A_p\sim47$, can be argued in the face of these smooth trends in spallation systematics. The consistency evident in all results is part of the argument. But another essential rationale focuses on inclusion of $A_p\sim72$ data as illustrated in Fig. 1. Lack of a smooth extrapolation between these product regions would require a discontinuity of $Y(A)$ somewhere between the two product regions. For an ^{89}Y target, for example, a hypothetical change in logarithmic slope would occur for products with ΔA somewhere in

TABLE III. Equation (1) fitted shape parameters from $A_p=47$ isobaric yield curves.

Target	P_0	μ_1	$(\mu_2')^{1/2}(10^{-2})$	$\mu_3'(10^{-4})$
^{89}Y($N/Z=1.282$)	1243± 16	1.154± 0.001	5.377±0.004	0.920± 0.059
^{92}Mo($N/Z=1.190$)	951± 11	1.141± 0.002	5.157± 0.003	0.804± 0.044
^{96}Mo($N/Z=1.286$)	588± 28	1.154± 0.001	5.420± 0.014	1.080± 0.220
^{100}Mo($N/Z=1.381$)	372± 20	1.167± 0.003	5.727± 0.021	1.440± 0.361
^{130}Te($N/Z=1.500$)	71.1± 4.5	1.171± 0.004	6.395± 0.034	2.011± 0.815

the range 17–42. But complementary measured yields of $A \sim 72$ products from targets covering this ΔA region give no evidence of any such variation in slope. A mechanism that retains a long-chain memory effect is consistent with the importance of emission of large fragments in the cascade and evaporation steps [10].

Since our shape parameters are derived from deep spallation data, it is legitimate to question how similar our results are to those for $A=47$ produced from less deep spallation ($\Delta A \leq 40$). We investigated this point by comparing the shape parameters from Table III with shape parameters derived from other published cross section data, the references for which are listed in Table IV, also fit to Eq. (1). Cross sections were corrected to the $A_p=47$ isobaric curve using mass-yield corrections similar to those used in the present study. Mass-yield coefficients were obtained (a) directly from the original publications, (b) by estimates from a linear regression of the experimental data, or (c) using interpolations from a mass-yield curve provided by Cumming *et al.* [38].

The most probable $A=47$ product compositions, as a function of target composition, $(N/Z)_T$, are represented in Fig. 4(a) as open circles. Similar to our very deep spallation results (solid circles), a product composition dependence on the target composition is evident. For example, the most neutron-deficient target, ^{58}Ni, has the most neutron-deficient product composition. Likewise, the more neutron-excessive targets La, Ta, and Au correspond to the more neutron-excessive product distributions. It is understood that the latter heavy targets might have appreciable contributions of neutron-excess products from high-energy fission. This was the rationale for choosing ^{130}Te to be the representative of neutron richness in a target in the current work.

The trends of the present study's data may be seen more clearly with the inclusion of the best linear fit of the current data (solid circles) represented by the solid lines. The slope of the line in Fig. 4(a) is 0.0997, which indicates that the spallation mechanism retains information on target composition over a range of mass loss including very deep spallation. Indeed, even stronger dependence of charge distribution on target composition is observed in production of heavier products for which the mass-energy surface is relatively steeply inclined [9,10,34,35,44,45]. For instance, Tobin and Karol [10] reported a slope of 0.279 for the dependence of $(N/Z)_p$ on $(N/Z)_T$ for $A_p=72$ isobaric distributions produced by 0.8 GeV protons on Y, Mo, and Te targets. Ku and Karol [9] reported the equivalent slope of 0.29 for the reactions of 0.72 GeV alphas with ^{92,96,100}Mo targets. Asano *et al.* [34] reported 0.304 from the reactions of 12 GeV protons with Zn, Cu, Ni, Co, and Fe targets to produce $A_p=50$ isobaric distributions.

We reanalyzed Sc spallation data published by Hagebø and Ravn [42], from the interactions of 18.2 GeV protons with Y, La, Ta, and Au targets, in which ΔA is approximately 42, 92, 134, and 150, respectively. A slope of 0.097 resulted from a linear regression of just this data alone. This value compares very favorably with 0.0997, the slope derived from our data, despite the increasing probability of a fission contribution in the heavier targets, especially at the higher bombarding energy.

In regard to the various semiempirical formulations, Rudstam's original expression would yield a horizontal straight line at $(N/Z)_p \sim 1.154$. The semiempirically derived slopes of 0.259 from the Chackett-Chackett expression (dot-dot-dashed line) and 0.213 derived from the expression of Silberberg *et al.* (dashed line) compare more favorably to the slopes derived from the less-deep spallation data leading to heavier products as reported by others [10,34,35]. These observations are not surprising since these formulas are based on abundant spallation systematics with cascade/evaporation chain lengths much shorter than $\Delta A=40$.

Similar trends can be observed in Figs. 4(b) and 4(c), which show target composition effects on the width and skewness of $A_p=47$ isobaric distributions. Overall, a shift to wider and more neutron-excess skewed distributions is observed as the target composition becomes more neutron excessive. As shown in Fig. 4, the semiempirically [24,30–32] derived isobaric distributions are mostly

TABLE IV. References for data in Figs. 4(a)–4(c).

12 GeV ^{1}H+^{nat}Ni, ^{59}Co, ^{nat}Zn, ^{nat}Fe, ^{nat}Cu	Asano *et al.* [34]
12 GeV ^{1}H+^{56,57}Fe, ^{58,60}Ni, ^{63,65}Cu	Noguchi *et al.* [35]
3.65 GeV ^{1}H+^{58,60}Ni, ^{63,65}Cu	Kozma, Tumendemberel, and Chultem [36]
3.65 GeV ^{1}H+^{55}Mn, ^{59}Co, ^{nat}Ni, ^{nat}Cu	Kozma, Ilyushchenko, and Hnatovicz [37]
3.9 GeV ^{1}H+^{nat}Cu	Cumming *et al.* [38]
24 GeV ^{1}H+^{nat}Cu	Rudstam, Brunnix, and Pappas [39]
28 GeV ^{1}H+^{nat}Cu	Cumming [20]
3, 29 GeV ^{1}H+^{nat}Ag	Katcoff, Fickel, and Wyttenbach [40]
300 GeV ^{1}H+^{nat}Ag	Porile, Cole, and Rudy [41]
18.2 GeV ^{1}H+^{89}Y, ^{140}La, ^{181}Ta, ^{197}Au	Hagebø and Ravn [42]
0.59 GeV ^{1}H+^{nat}As	Rudstam and Brunnix [43]

shape invariant with respect to target composition. The Rudstam [24] expression yields an invariant curve width $\sigma \sim 0.045$, appearing as a dotted line in Fig. 4(b). The expressions of Chackett and Chackett [30] and Silberberg *et al.* [31,32] show curve widths increasing somewhat with greater neutron excess in the target, although both underestimate the magnitude of this effect, especially in the more neutron-excess targets. It should be noted, though, that Sümmerer *et al.* [29], in their heavy-ion study, claim to see no evidence for a dependence of the product distribution width on target composition.

Some discussion of expected behavior of the dispersion of the isobaric distribution is worthwhile. The observed lack of symmetry in individual charge distribution curves is a signature of opposing trends in neutron and proton separation energies away from stability on the mass-energy surface. At late evaporation stages, under the influence of the Coulomb barriers to charged-particle emission, the spallation product distributions become neutron deficient. This behavior is constrained, however, as the proton dripline is approached. High neutron separation energies and low proton separation energies here severely reduce the competitiveness of neutron evaporation. Thus the steep, almost invariant slope of the neutron-deficient wings of the isobaric charge distributions mirror the effect of the mass-energy surface on evaporation. In contrast, spallation product distributions do not extend very far into the neutron-excessive domain on the other side of stability. Therefore spallation products on the neutron-rich side of the distribution are still quite remote from the influence of the proton/neutron separation energy imbalance implicit in the neutron-dripline extreme. As a result, the observed neutron-rich spallation products are less influenced by the mass-energy surface than their proton-rich counterparts and retain their sensitivities to target composition. This is witnessed experimentally in (i) the shifts, at constant A_p, of the peak widths and their increasing asymmetries in neutron-rich targets that lead to neutron-rich cascade residuals and also by (ii) the general increase in the curve widths as the product mass gets larger, reflecting the broadening of the nuclear mass-energy stability valley with A.

C. Very deep spallation

The conventional spallation model divides the reaction mechanism into two phases. First, the projectile strikes the target nucleus and causes the ejection of a number of particles by direct, fast cascading interactions. Then the struck, excited target residue relaxes by particle evaporation. Most recently, the model of Abul-Magd, Friedman and Hüfner [6] has reproduced the general features of spallation with this picture. Details of nuclear structure were intentionally omitted since those authors' objective was to understand the gross behavior of high-energy reactions. Because those gross features are entirely consistent with the two-step mechanism, one is encouraged to expect that more detailed consideration would provide further insight into the physics of the spallation process. We have been exploring features whose results appear to be qualitatively at odds with the mechanism as currently envisioned. Among the inconsistencies are the observations by Kaufman [46] and Tobin and Karol [10]. In the former, modest yields of high-energy very deep spallation products from ^{197}Au were difficult to reconcile with recoil momenta that implied low excitation energies of intermediate cascade residues. In the latter reference, anomalously and consistently high forward-to-backward recoil ratios for neutron-deficient spallation products compared to near-stable products from a medium mass target could not be accounted for within the standard mechanism.

The targets studied in this work ranged in composition from the neutron-deficient ^{92}Mo ($N/Z = 1.190$) to the neutron-excessive ^{130}Te ($N/Z = 1.500$). In the dynamic excitation phase leading to residues at least several mass numbers removed from the target, the relative ejection probabilities of neutrons and protons vary quite regularly with target composition [9,10,22,28]; that is, initial N/Z differences between the target nuclei are retained by the cascade step [25,28]. This is the foundation of the spallation yield "memory effect."

Subsequent particle emission probabilities are governed by the location of the cooling nucleus with respect to nuclear stability on the mass-energy surface [8], i.e., both the location of the stability valley and relative separation energies of evaporated particles. Separation energies strongly influence the competitive emission rates of protons and neutrons, funneling the cooling nuclei toward stability. The products studied in this effort had $41 \leq \Delta A \leq 87$. Even if we hypothetically viewed the entire 0.8 GeV incident energy as available for evaporation with ~ 10 MeV energy loss per nucleon (a couple of MeV above average separation energy), we are qualitatively at the limit of evaporative emission. In fact, Abul-Magd, Friedman, and Hüfner [6] showed that the average energy carried away per unit evaporative mass loss was ~ 13 MeV. Long evaporation chains such as those leading to our observed very deep spallation products should, according to the model, converge, decreasing for the most part any differences that arose from initial cascade composition [29]. Neutron-rich cascade residuals from ^{130}Te, for example, would preferentially evaporate neutrons since separation energies for neutrons would be much lower than for protons in such residuals. Near the very end of the cooling process, the Coulomb barrier increasingly inhibits charged-particle emission rates, eventually shifting product distributions toward the neutron-deficient side of stability.

However, despite expectations that a large number of evaporation steps should wash out memory of initial target composition, the product distributions in our very deep spallation results nevertheless continue to reflect a significant effect of target N/Z. Figures 2(a)–2(f) show a clear drift in the distribution peak positions toward increasing N/Z with the more neutron-rich targets. One simple explanation lies in the *substantial* role assigned to the ejection of large clusters during the cascade process. This is a path usually neglected in spallation analysis. Although its influence is still speculative, there is accumulating circumstantial evidence [10,46–48] that such cluster ejections are a reasonable and necessary facet in

the formation of spallation products in intermediate and high-energy reactions.

V. CONCLUSIONS

Yields of Sc radioisotopes from the interaction of 0.8 GeV protons with ^{89}Y, ^{92,96,100}Mo, and ^{130}Te targets were measured. Aided by established spallation systematics, the yields from each target were used to generate "$A=47$ isobaric distribution curves." Mass yields constructed from the isobaric distributions were compared to mass yields determined previously [10] at $A\sim72$ from the same targets. The exponential decrease in product mass yields with increasing mass loss from all of the targets was observed to be preserved into the very deep spallation region. A precise parametrization of the curves clearly showed a regular dependence of the shape parameters (mean, width, and skewness) with target composition indicating the "memory" effect persists at even very large mass losses, $\Delta A\sim85$. Persistence of the memory effect argues for the importance of cluster ejection and evaporation, something still downplayed in most calculations.

The isobaric curves and mass yields were compared to several widely used semiempirical parametrizations. All of those formulas seriously underestimate the widths of the isobaric distributions, fail to account for the asymmetric shapes of the isobaric curves, and cannot reproduce the experimentally observed shifts in widths with increasing neutron excess in the target. While adequately estimating the mass yields in the deep spallation mass region from the ^{89}Y and ^{92,96,100}Mo targets, $46\leq\Delta A\leq57$, the semiempirical formulas do not reproduce, within an order of magnitude, the very deep spallation mass yields from ^{130}Te, $\Delta A\sim85$.

ACKNOWLEDGMENTS

The authors are grateful to LAMPF for the use of their facilities. In particular, the assistance of Dr. B. J. Dropesky, Dr. L. C. Liu, and Dr. G. C. Giesler was appreciated. Discussions with colleagues at Carnegie Mellon University were also helpful, especially those with Dr. M. J. Tobin. The financial support of the Department of Energy is also acknowledged. Dr. K. L. Kolsky submitted this work in partial fulfillment of the Ph.D. degree, Department of Chemistry, Carnegie Mellon University.

[1] V. F. Weiskopf, Phys. Rev. **52**, 295 (1937).
[2] R. Serber, Phys. Rev. **72**, 1114 (1947).
[3] H. Nifenecker and J. A. Pinston, Annu. Rev. Nucl. Part. Sci. **40**, 113 (1990).
[4] S. Kox, A. Gamp, R. Cherkaoui, A. J. Cole, N. Longequeue, J. Menet, C. Perrin, and J. B. Viano, Nucl. Phys. **A420**, 162 (1984).
[5] L. Winsberg, Phys. Rev. C **22**, 2116 (1980).
[6] A. Y. Abul-Magd, W. A. Friedman, and J. Hüfner, Phys. Rev. C **34**, 113 (1986).
[7] J. Hüfner, Phys. Rep. **125**, 129 (1985).
[8] K. LeCouteur, Proc. Phys. Soc. (London) A **63**, 259 (1950); **65**, 718 (1952).
[9] T. H. Ku and P. J. Karol, Phys. Rev. C **16**, 1984 (1977).
[10] M. J. Tobin and P. J. Karol, Phys. Rev. C **39**, 2330 (1989).
[11] W. R. Webber, J. C. Kish, and D. A. Schrier, Phys. Rev. C **41**, 520 (1990); **41**, 533 (1990); **41**, 547 (1990); **41**, 566 (1990).
[12] G. Andersson, M. Areskoug, H. A. Gustafsson, G. Hylten, B. Schroder, and E. Hagebø, Phys. Lett. **71B**, 279 (1977).
[13] M. J. Tobin, Ph.D. dissertation, Carnegie Mellon University, 1986; T. Ku and P. J. Karol, Nucl. Instrum. Methods **121**, 537 (1974).
[14] S. Shibata (private communication).
[15] C. M. Lederer and V. S. Shirley, *Table of Isotopes,* 7th ed. (Wiley, New York, 1978).
[16] J. B. Cumming, in *Application of Computers to Nuclear and Radiochemistry,* edited by G. D. O'Kelley, National Academy of Science, Nuclear Science Series NAS-NS-3107 (Office of Technical Services, Washington, D.C., 1963).
[17] S. G. Lindqvist, The Swedish University of Åbo, Finland, Computer Center Report No. 9, 1981.
[18] A. R. Eherle and M. W. Lerner, Anal. Chem. **27**, 1551 (1955).
[19] K. L. Kosky, Ph.D. dissertation, Carnegie Mellon University, 1989.
[20] J. B. Cumming, Annu. Rev. Nucl. Sci. **13**, 261 (1963).
[21] J. B. Cumming, R. W. Stoenner, and P. E. Haustein, Phys. Rev. C **14**, 1554 (1976).
[22] P. J. Karol, Phys. Rev. C **10**, 150 (1974).
[23] R. von Mises, in *Mathematical Theory of Probability and Statistics,* edited by H. Geiringer (Academic, New York, 1964).
[24] G. Rudstam, Z. Naturforsch. **21A**, 1027 (1966).
[25] N. T. Porile and L. B. Church, Phys. Rev. **133**, B310 (1964).
[26] C. Thibault-Philippe, Ph.D. dissertation, University of Paris, Report No. CNRS A05862, 1971.
[27] G. Friedlander, J. W. Kennedy, E. S. Macias, and J. M. Miller, *Nuclear and Radiochemistry,* 3rd ed. (Wiley, New York, 1981).
[28] J. M. Miller, in *High-Energy Nuclear Reactions in Astrophysics,* edited by B. S. Shen (Benjamin, New York, 1968).
[29] K. Sümmerer, W. Brüchle, D. J. Morrissey, M. Schädel, B. Szweryn, and Y. Weifan, Phys. Rev. C **42**, 2546 (1990).
[30] K. F. Chackett and G. A. Chackett, Nucl. Phys. **A100**, 633 (1967).
[31] R. Silberberg and C. H. Tsao, Astrophys. J. Suppl. **25**, 313 (1973); **25**, 335 (1973).
[32] R. Silberberg, C. H. Tsao, J. R. Letaw, and M. M. Shapiro, in *Genesis and Propagation of Cosmic Rays,* Vol. 220 of *NATO Advanced Study Institute, Series B: Physics,* edited by M. M. Shapiro and J. P. Wefel (Reidel, Dordrecht, Holland, 1988).
[33] J. T. Routti and J. V. Sandberg, Comput. Phys. Commun. **23**, 411 (1981).
[34] T. Asano *et al.*, Phys. Rev. C **28**, 1718 (1983).
[35] M. Noguchi, H. Hirabayashi, K. Katoh, K. Kondo, and M. Takasaki, Phys. Rev. C **38**, 1811 (1988).
[36] P. Kozma, B. Tumendemberel, and D. Chultem, Czech. J. Phys. **40**, 29 (1990).

[37] P. Kozma, V. I. Ilyushchenko, and V. Hnatovicz, Yad. Fiz. **53**, 722 (1991) [Sov. J. Nucl. Phys. **53**, 451 (1991)].
[38] J. B. Cumming, P. E. Haustein, R. W. Stoenner, L. Mausner, and R. Naumann, Phys. Rev. C **10**, 739 (1974).
[39] G. Rudstam, E. Brunnix, and A. C. Pappas, Phys. Rev. **126**, 1852 (1962).
[40] S. Katcoff, H. Fickel, and A. Wyttenbach, Phys. Rev. **166**, 1147 (1968).
[41] N. T. Porile, G. D. Cole, and C. R. Rudy, Phys. Rev. C **19**, 2288 (1979).
[42] E. Hagebø and H. Ravn, J. Inorg. Nucl. Chem. **31**, 897 (1969).
[43] G. Rudstam and E. Brunnix, J. Inorg. Nucl. Chem. **23**, 161 (1961).
[44] S. Regnier, Ph.D. dissertation, The University of Bordeaux, 1977.
[45] M. Lagarde-Simonoff, S. Regnier, H. Sauvageon, and G. N. Simonoff, Nucl. Phys. **A260**, 369 (1976).
[46] S. B. Kaufman, Phys. Rev. **129**, 1866 (1963).
[47] M. J. Tobin and P. J. Karol, Phys. Rev. C **38**, 267 (1988).
[48] R. E. L. Green, R. G. Korteling, and K. P. Jackson, Phys. Rev. C **29**, 1806 (1984).